THE INFLUENCE OF TUNNEL DEFORMATION PATTERNS ON SURFACE SETTLEMENT: A CASE STUDY

Gang Niu[1], Shaoheng Dai[1], Yunhan Wang[2], Haoding Xu[3] and Xuzhen He[1]

[1]University of Technology Sydney, Australia; [2]Shandong Jiaotong University, China;
[3] Xi'an University of Technology, China

https://doi.org/10.56295/AG6113

ABSTRACT

Tunnelling-induced ground surface settlement (GSS) poses potential risks to buildings and underground utilities in urban areas. Commonly used approaches for GSS assessment, including three-dimensional (3D) numerical simulations and artificial intelligence techniques, are often limited by high computational costs or poor generalizability. To overcome these limitations, this study proposes a simplified and efficient two-dimensional (2D) numerical method for rapid estimation of GSS at different tunnel cross-sections. The approach replaces the detailed 3D step-by-step excavation processes by employing 2D plane strain conditions, while incorporating convergence patterns characterized by the gap parameter (g) and volume loss (V_L). Several typical tunnel deformation models are numerically analysed to evaluate their influence on the resulting settlement troughs. The results demonstrate that the proposed method can effectively capture key GSS characteristics while improving computational efficiency. In addition, this method enables probabilistic analysis in the absence of comprehensive field data, supporting early design decisions. Future research can further refine this approach by incorporating more advanced soil constitutive models and considering tunnel–soil interaction effects to improve the accuracy of GSS evaluation.

1. INTRODUCTION

Urbanization in recent years has increased the need for underground space utilization. Tunnel construction offers an effective solution to alleviate traffic congestion (Song et al., 2023, Yan et al., 2023). However, the settlement of ground surface induced by tunnelling is a crucial concern in urban area, as it can impact the structural integrity of surface buildings and infrastructure (Franza et al., 2019; Huang et al., 2022; Chen et al., 2024).

There are many methods that have been proposed for tunnelling-induced GSS analysis, including empirical, analytical, numerical and artificial intelligence methods. Empirical methods, which can provide a brief estimation of GSS, are based on field observations and engineering experience (Islam and Iskander, 2021; Tang and Na, 2021). Analytical solutions, including Loganathan and Poulos (1998), Verruijt and Booker (1996), Park (2005), Zhang et al. (2011), Zhang and Huang (2012), Zareifard (2019), Zhu et al. (2023), Cao et al., (2024) and so on, offer a preliminary evaluation of GSS. These analytical methods either rely on the elasticity theory or provide complex formulas. Some important soil parameters such as cohesion and friction angle are overlooked, and the nonlinear elastic behavior of soil is neglected. Consequently, both empirical and analytical methods fail to precisely represent tunnelling-induced GSS across diverse geotechnical conditions and tunnel projects (Hussaine and Mu, 2022; Kim et al., 2022; Tang and Na, 2021; Zhang et al., 2020; Zhou et al., 2024). Many machine learning approaches, such as artificial neutral network (Boubou et al., 2010; Chen et al., 2019; Moghaddasi and Noorian-Bidgoli, 2018; Pourtaghi and Lotfollahi-Yaghin, 2012; Zhang et al., 2020), recurrent neutral network (Mahmoodzadeh et al., 2020; Zhang et al., 2020) and random forest (Huang et al., 2023; Ling et al., 2022; Liu et al., 2022), have been proposed to predict GSS caused by tunnelling using soil properties and tunnel boring machine (TBM) operation parameters as inputs. However, the generalization ability of machine learning models is often restricted, which means the trained machine learning models are only applicable to individual tunnel projects due to limitation of training data.

Numerical simulation is another effective tool capable of assessing GSS across a diverse range of geotechnical conditions. Finite Element Method (FEM) and Finite Difference Method (FDM) have been widely adopted to analyse tunnelling activities and the resulting GSS. In numerical simulations, step-by-step simulation of tunnel excavation is the most popular approach (Niu et al., 2023; Santos and Celestino, 2008). These simulations generally show good agreement with field measurements. However, step-by-step simulation of tunnelling activities is time-costing and resource-intensive. Establishing 3D numerical model and simulating tunnelling process by multiple steps repeatedly are relatively complicated. For different tunnelling methods, such as sequential excavation, drilling and blasting, tunnelling under the

protection of shield and TBM methods, it is difficult to employ a numerical simulation model to deal with all situations. Furthermore, in the 3D approach, GSS is affected by many factors, such as face pressure, grouting pressure, grouting consolidation, excavation speed, stoppage etc., where these parameters are not well known before tunnelling, as TBM operation parameters depend on geotechnical conditions and need to be adjusted dynamically (Dias and Kastner, 2013). As a result, 3D simulation of tunnelling process generally concentrates on back-analysis (Miro et al., 2015; Russo et al., 2015). In addition, tunnels do not always maintain a horizontal trajectory but may curve or move up and down (Shen et al., 2022; Hu, et al., 2024). However, 3D numerical simulations usually focus on a specific distance of tunnel excavation, assuming constant tunnel depth and uniform distribution of soil layers along this distance. Geotechnical variability (e.g. soil layers distribution, ground properties), tunnelling parameter fluctuations (e.g. advancement speed, grouting pressure), and tunnel geometry complexity (e.g. tunnel depth, tunnelling direction) also challenge full length 3D tunnelling simulations.

Because of simplicity, 2D simulation of tunnelling activities has been widely adopted, with many methods proposed such as gap method (Rowe et al., 1983), convergence confinement method (Paraskevopoulou and Diederichs, 2018), stress reduction method (Möller and Vermeer, 2008), displacement-controlled method (Cheng et al., 2007; Do et al., 2014; Hejazi et al., 2008; Ma et al., 2018), volume loss control method (Shiau and Sams, 2019) and so on. These approaches aim to study GSS by analysing tunnel profile deformation along tunnel cross-sections. However, the simulation result is significantly sensitive to some specific parameters that are difficult to determine, such as the stress relaxation coefficient. In addition, the proposed tunnel convergence patterns are not comprehensive and need further exploration.

To solve these problems, this study employs 2D numerical model for analysis of tunnelling-induced GSS, by simplifying the complex tunnel excavation processes into different tunnel convergence models using the displacement-controlled method (DCM). The significance and practical value of this study is that GSS trough can be estimated at the early stages of a tunnel project using limited data such as geotechnical properties, tunnel geometry, and tunnel convergence parameters (g or V_L). On the other hand, for back-analysis, this approach also enables the probabilistic assessment of transverse GSS troughs at different tunnel cross-sections.

As shown in Figure 1, the structure of this paper is organized as follows. Section 2 explains GSS principle and indicates commonly used parameters for the assessment of the GSS problem. Section 3 reviews DCM and proposes some tunnel convergence models based on the g or V_L, respectively. The corresponding tunnel convergence functions for each model are derived and presented. Section 4 uses case studies to verify the effectiveness of the introduced method by comparing the simulation results with field data. The parametric study is conducted in Section 5, clarifying the relationships of the maximum GSS (S_{max}) with tunnel depth (H), tunnel diameter (D), gap parameter (g) and volume loss (V_L). In Section 6, the advantages and limitations of this study are discussed, with future improvements suggested.

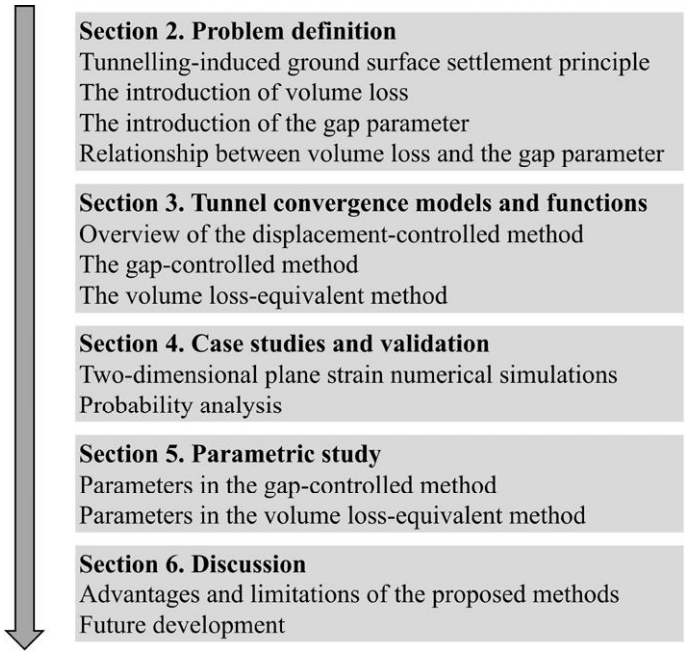

Figure 1: The workflow diagram of this study.

2. PROBLEM DEFINITION

As shown in Figure 2, the tunnelling activity disturbs the geostatic balance, causing the surrounding soil to move inward toward the tunnel, which results in the finished area being smaller than the excavated area. This phenomenon is known as volume loss, which describes the difference between the excavated tunnel area and the planned tunnel area. It is calculated by taking the difference between the actual excavated volume and the planned volume, and dividing this by the planned tunnel volume. Factors such as geotechnical properties, tunnelling method, and tunnel geometry can significantly influence the magnitude of volume loss (Golpasand et al., 2016; Niu et al., 2023; Vu et al., 2016).

Generally, the space created between the tunnel boundary and the lining is filled by collapsing soil from above the tunnel. This soil displacement leads to localized ground movement and GSS (see Figure 2). The void, particularly at the tunnel crown, represents the physical distance between the excavated tunnel boundary and the lining, playing a critical role in determining the magnitude of GSS. Larger voids cause more significant GSS due to increased soil collapse. The gap parameter indicates the size of this void, reflecting the potential extent of soil collapse and displacement, and indirectly represents the magnitude of volume loss.

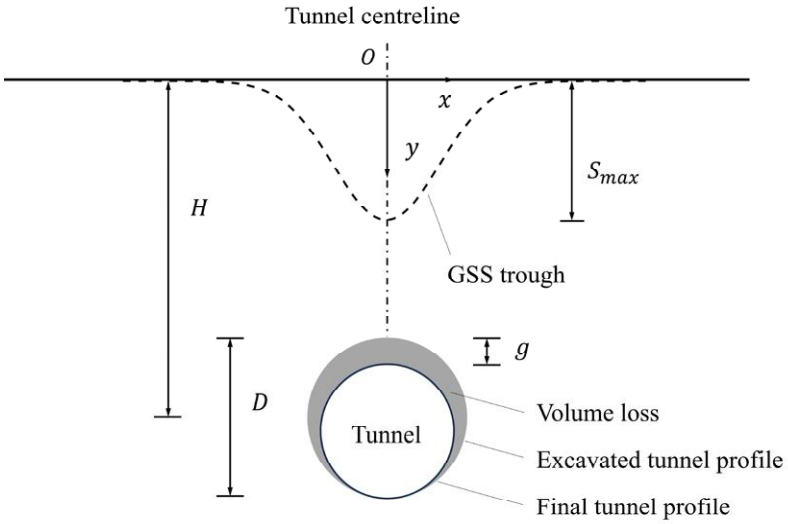

Figure 2: An illustration of tunnelling-induced ground movement and surface settlement.

The g and V_L are two important indicators for assessing the stability and safety of the liner as well as evaluating tunnelling-induced GSS (Jallow et al., 2019; Lin et al., 2021; Zakhem and El Naggar, 2019). They can be determined through back-analysis utilizing monitoring data and appropriate modelling techniques. To obtain g, one method is to measure the settlement of the tunnel crown at construction site directly. This is relatively different for TBM constructed tunnel (Xie et al., 2021). Lee et al. (1992) proposed that g depends on TBM tail void and the quality of workmanship. Zhu and Li (2017) conducted a more detailed investigation into this parameter and identified six key contributing factors. Another approach involves fitting the measured GSS data with a Gaussian curve to estimate g. By analysing the width and depth of GSS trough and correlating it with H and D, g can be inferred. The same condition applies to V_L. The fitted Gaussian curve can be used to evaluate the value of V_L. On the other hand, numerical methods can also assist in back-calculating V_L by adjusting model parameters until the simulated GSS trough closely matches field observations.

Loganathan and Poulos (1998) simplified the correlation between g and V_L (see Equation 1) and provided analytical solutions under the assumption that the converged tunnel maintains an ideal shape with its excavated profile. The g is defined as the maximum settlement of the tunnel crown during tunnelling (Cao et al., 2020).

$$g = 2R(\sqrt{V_L + 1} - 1) \quad (1)$$

3. DISPLACEMENT-CONTROLLED METHOD AND TUNNEL CONVERGENCE PATTERNS

GSS is primarily influenced by ground properties, tunnel geometry as well as excavation and support method (Niu et al., 2023; Santos and Celestino, 2008). These factors are reflected through tunnel convergence and ground loss, which is the main contributors to GSS in the short term (Feng et al., 2022). Other factors such as creep and consolidation of soil and thermal effect have limited contributions, as a result, they are often neglected in short-term GSS analysis (Le et al., 2023).

DCM is a method of implementing confinement forces or specified displacements to the tunnel wall (Do et al., 2014). It is widely used to simulate ground response due to tunnelling. For example, tunnelling process can be simply simulated through a uniform radial contraction of the excavated tunnel profile (Hejazi et al., 2008). This means tunnel contracts radially until the predefined ground loss is reached. In some conditions, the tail void grouting and subsequent consolidation phases can also be simulated by accounting for the variations in the excavation boundary to better represent real construction procedures. For example, grouting injection phase can be depicted by an increase in tunnel diameter, while the consolidation phase can be characterized by a subsequent reduction in tunnel diameter (Dias and Kastner, 2013). The simulation of grouting injection phase captures the immediate expansion of tunnel boundary due to grouting, while the consolidation phase reflects the long-term ground response that occurs after the grout hardens and excess pore pressures dissipates. However, in practise, tunnel convergence exhibits highly nonuniformity, with more crown settlement and less invert heave (Cheng et al., 2007; Zhang and Huang, 2012). It is reported that the nonuniform convergence patterns of tunnel can provide more realistic and accurate predictions of GSS (Park, 2005; Zhang and Huang, 2012).

Based on g and V_L, this study presents multiple typical tunnel convergence models to describe tunnel convergence characteristics and uses DCM to analyse the resultant GSS. Specifically, tunnel convergence functions are derived based on the assumed tunnel convergence patterns. These functions are then implemented in the finite element software ABAQUS to simulate the targeted deformation at the tunnel periphery. For these scenarios, the corresponding GSS troughs are obtained, and the area covered by these various GSS troughs represents the probabilistic GSS outcome.

3.1 GAP-CONTROLLED METHOD

The potential ground movement at the tunnel crown, referred as ‘gap’, is an important parameter for assessing tunnel convergence and resultant GSS. For tunnel constructed using TBM, the diameter excavated by cutterhead is always larger than the outer diameter of lining. The void between the excavated tunnel boundary and the lining outer skin is commonly filled with grouting injection, effectively minimizing the gap and reducing the GSS. The effectiveness of grouting depends on many factors, such as grouting pressure, grouting volume, soil permeability and the types of grouting materials used. Higher grouting pressure can enhance the filling of the void, thereby reducing GSS. However, excessive pressure can lead to grout overflow and destabilize the surrounding soil, potentially exacerbating deformations. In addition, the grouting volume should be adequate to fill the void, while soil permeability influences the ability of grouting material to spread and bond effectively with the surrounding soils. The selection of grout type is also crucial, as it should be suited to the specific soil conditions. For example, high-flow grouts are ideal for permeable soils to ensure proper filling of voids, while fast-setting grouts are used in areas with high water inflow to provide rapid stabilization.

There are multiple methods for the evaluation of g. For example, Lee et al. (1992) proposed the following equation for calculating g.

$$g = G_P + U_{3D}^* + \omega \tag{2}$$

Where G_P is the physical gap which is the distance between the excavated tunnel boundary and outer skin of the lining, U_{3D}^* is the 3D elastoplastic deformation at the tunnel face, ω is the workman factor. The determination of these parameters can refer to Loganathan and Poulos (1998), Chakeri et al. (2013), Chi et al. (2001), Yang et al. (2021) and Yang et al. (2022).

Zhu and Li (2017) further studied this parameter, identifying six primary contributing factors. These include the face pressure at tunnel face, the grouting effect, the supporting pressure between surrounding soil and liner, yawing and pitching of TBM, and the long-term volume loss of disturbed soil. The estimation of these factors (gap induced by inadequate shield support pressure, gap due to grouting, gap due to intermittent shield alignment, gap due to shield yawing, gap due to shield pitching and gap due to long term volume loss) can be found in Zhu and Li (2017) accordingly.

In the proposed gap-controlled method, while g at the tunnel crown remains constant, the effect of different tunnel ovalization degrees on the GSS is investigated. As presented in Figure 3, pattern one represents a uniform radial

contraction. Remaining patterns indicate more complex scenarios, taking into account the impacts of vertical movement and ovalization of the liner. The dashed lines represent the original shape of tunnel periphery after excavation, whereas the solid lines represent converged tunnel periphery. It should be noted that the gap configurations shown in Figure 3 are not unique and can vary under different ground conditions. Parameters such as the lateral earth pressure coefficient (K_0) and ground stiffness have a significant influence on the deformation mode of the tunnel periphery. For example, under a high K_0 condition, tunnel deformation is dominated by horizontal convergence due to the relatively larger in-situ horizontal stress. As a result, inward displacement is concentrated at the sidewalls, while vertical deformation at the crown and invert is comparatively restrained. The tunnel cross-section therefore tends to evolve toward a horizontally compressed and vertically elongated shape.

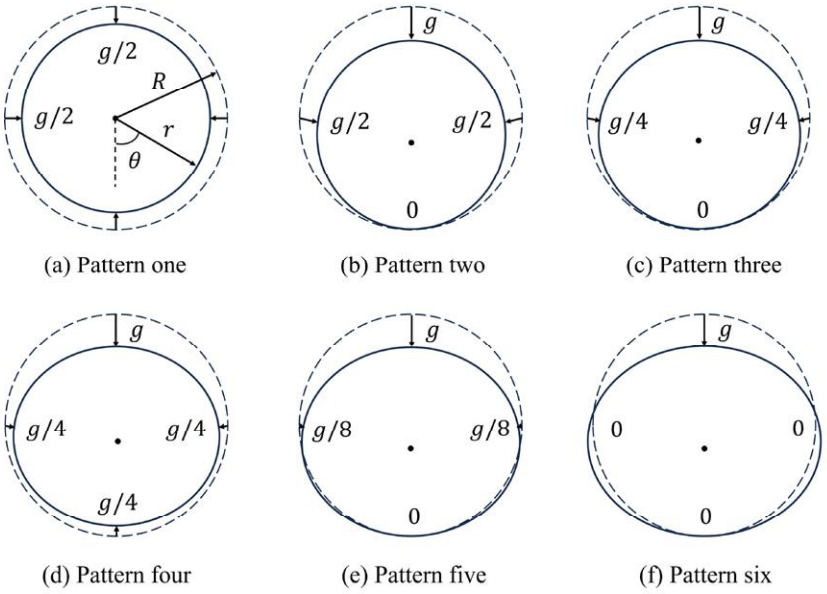

Figure 3: Illustration of gap-controlled method.

The boundary conditions corresponding to each pattern are listed as follows.

$$u_r(r = R) = -\frac{1}{2}g \tag{3}$$

$$u_r(r = R) = -\frac{1}{\pi}g\theta \tag{4}$$

$$u_r(r = R) = -\frac{1}{\pi^2}g\theta^2 \tag{5}$$

$$u_r(r = R) = -g(\frac{1.5}{\pi^2}\theta^2 - \frac{0.75}{\pi}\theta + \frac{1}{4}) \tag{6}$$

$$u_r(r = R) = -g(\frac{1.5}{\pi^2}\theta^2 - \frac{0.5}{\pi}\theta) \tag{7}$$

$$u_r(r = R) = -g(\frac{2}{\pi^2}\theta^2 - \frac{1}{\pi}\theta) \tag{8}$$

Where u_r is the boundary condition that represents the displacement magnitude along the tunnel periphery, R is non-deformed tunnel radius after excavation, g is gap parameter, r is radial coordinate in the cylindrical coordinate system and θ is angular coordinate (the angle counterclockwise from tunnel invert), ranging from 0 to π, as shown in Figure 3 (a).

3.2 VOLUME LOSS-EQUIVALENT METHOD

When quantifiable volume loss is calculated, an alternative approach named volume loss-equivalent method can be adopted, which focuses on the equivalent volume loss. It assumes that the tunnel liner maintains a similar shape after deformation. This method involves progressively lowering the converged tunnel periphery, step by step, to assess the resulting GSS (see Figure 4). Figure 4 (a) is the case of uniform radial contraction, while Figure 4 (f) represents the case that the invert of converged tunnel is tangent to its non-deformed shape. For other cases, a normalized parameter $g^{'}$ is used (presented in Equation 9), indicating the intermediate state of tunnel periphery convergence from the uniform contraction to the tangent case.

$$g^{'} = g_{new}/g \tag{9}$$

Where $g^{'}$ is normalized gap parameter, g_{new} represents the displacement of tunnel crown, g is gap parameter.

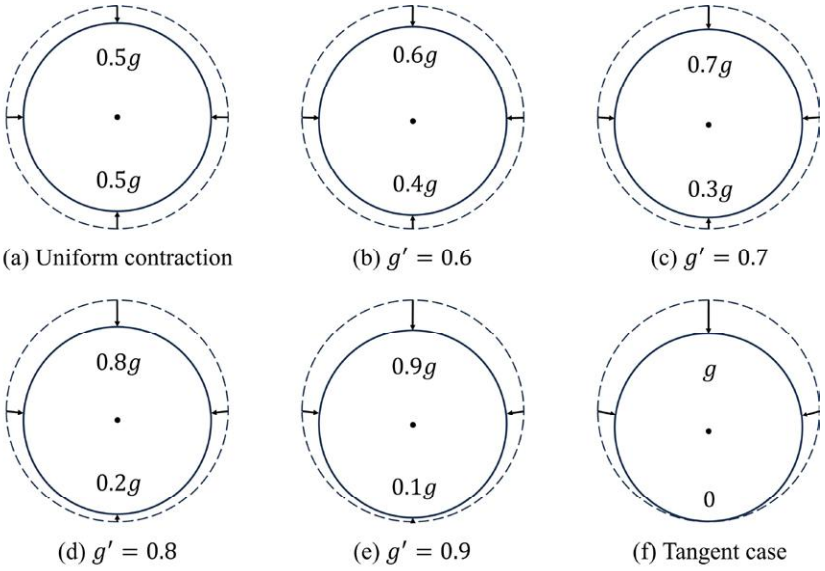

Figure 4: Illustration of volume loss-equivalent method.

The corresponding equations for each case are detailed as follows:

$$u_r(r = R) = -\frac{1}{2}g \tag{10}$$

$$u_r(r = R) = -g(\frac{0.2}{\pi}\theta + 0.4) \tag{11}$$

$$u_r(r = R) = -g(\frac{0.4}{\pi}\theta + 0.3) \tag{12}$$

$$u_r(r = R) = -g(\frac{0.6}{\pi}\theta + 0.2) \tag{13}$$

$$u_r(r = R) = -g(\frac{0.8}{\pi}\theta + 0.1) \tag{14}$$

$$u_r(r = R) = \frac{g}{\pi}\theta \tag{15}$$

4. CASE STUDIES

The effectiveness of the proposed methods is verified through case studies. In each case study, a 2D finite field is established, with its size determined based on literature (Jin et al., 2022; Shen et al., 2014). For example, it is suggested that the distance between tunnel invert and field bottom should be larger than one tunnel diameter to eliminate the potential influence of boundary conditions (Chen et al., 2013; Noubissi et al., 2024; Shahin et al., 2011; Shahin et al., 2019). Moreover, Mohr- Coulomb (MC) constitutive model is used to describe soil behaviors in all 2D plane strain simulations in this study.

The numerical simulation procedure mainly includes two steps:

(1) Applying gravity to all soil elements to achieve geostatic balance. The predefined stress field is established based on soil density and gravity acceleration (taking $g_0 = 10m/s^2$), with lateral earth pressure coefficient (K_0) assigned for each soil layer respectively.

(2) Deactivating soil elements within the tunnel periphery while applying displacement boundary conditions (as presented in Figure 3 and 4) to the tunnel periphery.

4.1. XI'AN METRO LINE 2

4.1.1 Background

Xi'an Metro Line 2 is located in Shanxi, China, constructed using Earth Pressure Balance Shield Machine (EPBSM). The excavation diameter of this tunnel is 6.16m, and the diameter of liner outer skin is 6.0m. It passes through silty clay deposits and old loess, with a buried depth varies from 12.6m to 22.4m. As the tunnel excavation proceeds, variations in soil properties, tunnel depth and volume loss are monitored, leading to variations in GSS at different sections. According to back-analysis from Zhu and Li (2017), Section 13+290, where the tunnel has a 14.2m axis depth with a 31.4mm gap parameter, is selected for detailed analysis in this study.

4.1.2 Geotechnical conditions

The soil composition surrounding the upper part of the tunnel consists of a mixture of fill, soft saturated loess, and new loess (Ma et al., 2016; Peng et al., 2017). Meanwhile, the soil around the lower part of the tunnel is mainly sandy soil (Lai et al., 2020). Physical and mechanical parameters of soil are mainly determined from laboratory triaxial compressibility tests. Based on laboratory experiments and engineering experience, Zhu and Li (2017) proposed the weighted average of physical and mechanical parameters for the soils around the tunnel (shown in Table 1).

Table 1: Soil parameters at Section 13+290 (Zhu and Li, 2017).

Parameter, symbols and unit	Value
Unit weight γ, kN/m^3	19.0
Cohesion c, kPa	27.6
Friction angle φ, °	26.4
Young's modulus E, MPa	31.5
Poisson's ratio v	0.383
Earth pressure at rest K_0	0.62

4.1.3 Model establishment

The numerical simulation model is shown in Figure 5, where the field size is 28.4m in height and 100m in width. Centre of tunnel is located at approximately 14.2m depth with an equivalent 6.16m excavation diameter. For boundary conditions, the base of the field is fixed, ensuring no vertical or horizontal displacement occurs at the bottom boundary. Both lateral sides are treated as rollers, allowing vertical movement but restraining horizontal displacement. The size of square element (CPE4R) is 0.5m, which is densified in the region surrounding the tunnel. In this case, a total of 11560 elements with 11817 nodes is generated in ABAQUS.

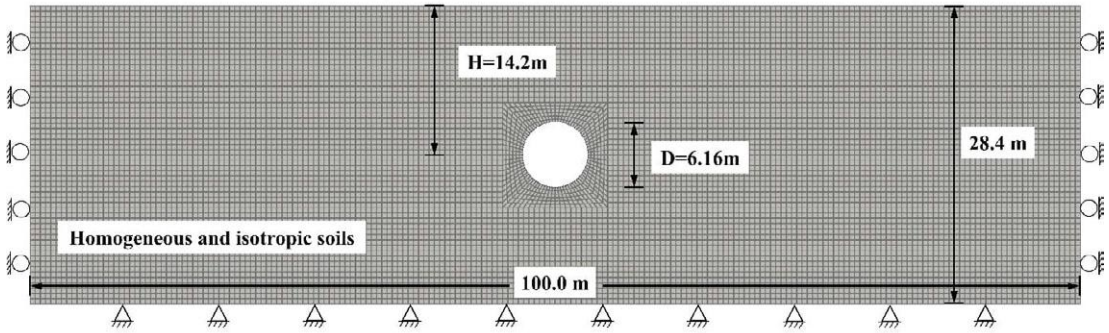

Figure 5: Setup of 2D numerical simulation model of Xi'an Metro Line 2.

4.1.4 Results

Keeping g at the tunnel crown constant, different tunnel convergence patterns due to ovalization are studied. Based on Equation 3 to 8 and Figure 3, the gained numerical simulation results are compared with field measurements (see Figure 6). As can be illustrated, GSS trough obtained from FEM is in good agreement with in-situ observations, both in shape and magnitude. Results also indicate that the uniform radial contraction pattern (pattern 1 in Figure 3) cannot reflect GSS trough accurately. Since tunnel geometry is symmetrical while the loading acting on tunnel periphery is not, the assumption of uniform contraction around tunnel periphery is over-ideal. As a result, it cannot accurately represent the actual tunnel convergence behaviors in reality. On the other hand, pattern 2, which is characterized by the invert of converged tunnel aligning tangentially with that of the excavated tunnel, tends to over-estimate GSS trough. This is consistent with field observations that the invert of excavated tunnel commonly experience heave. Since tunnel excavation releases the stresses in the surrounding soil, the redistribution of stress can lead to a reduction in compressive stress within the stratum, leading to the convergence of tunnel periphery such as settlement of the crown and heave of the invert.

In addition, Figure 6 also indicates that the non-uniform tunnel convergence patterns (pattern 3, 4, 5 and 6) can provide more precise GSS trough estimation. The g value has significant influence on the maximum GSS. As this parameter is ensured, the variation of the maximum GSS is limited. The dark grey region depicts the state of GSS trough resulted from no tunnel springline displacement (pattern 6) to large springline movement (pattern 2), representing the area of higher probability of GSS occurrence. For the light grey region, it corresponds to area where GSS results from uniform convergence of tunnel periphery (pattern 1) to no movement of tunnel springline (pattern 6), indicating a lower probability of GSS occurrence.

The shapes and slopes of GSS trough are also crucial in assessing the impact of tunnelling on adjacent structures. While the maximum GSS indicates the extent of ground movement, the slopes of the trough reveal the pattern of settlement distribution across the affected area. Steeper slopes can create sharper gradients of ground deformation, increasing the risk of structural damage to nearby buildings, utilities, and infrastructure due to differential settlement. In contrast, broader and gentler slopes indicate a more gradual transition in ground deformation, typically resulting in less severe structural impacts.

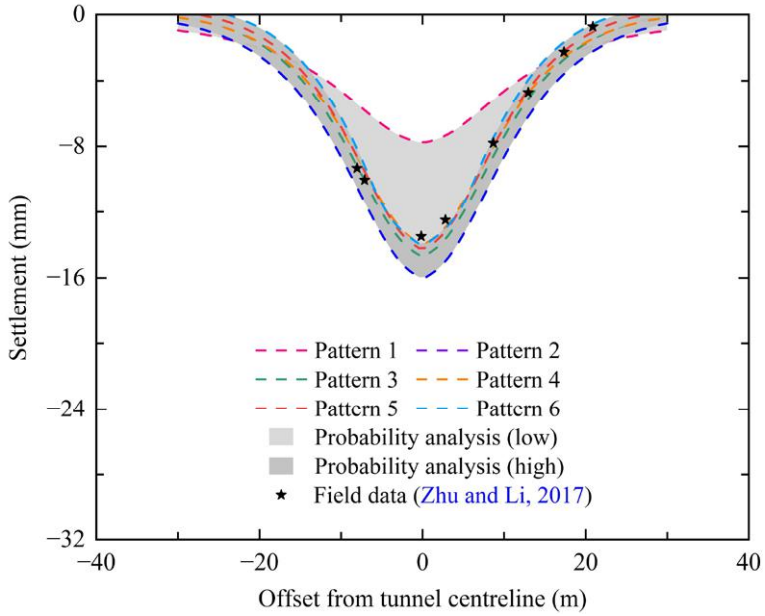

Figure 6: Transverse ground surface settlement of Xi'an Metro Line 2 Section 13+290.

4.2 MILAN METRO LINE 1

4.2.1 Background

The Milan underground Line 1 is constructed in alluvial sandy area of Padana Plain, using EPBSM. Tunnel depth varies between 8 and 19 meters beneath ground surface. Featuring a cutter head diameter of approximately 6.54m, the tunnel is lined with segments having an outer diameter of 6.3m and a thickness of 0.3m. The space between the excavated wall and outer skin diameter of the lining is filled with grout injection. During tunnelling process, variation of H, V_L and S_{max} are monitored at different cross-sections along tunnel length (Migliazza et al., 2009). Based on field measurements from Migliazza et al. (2009), a cross-section with 13.5m depth and 0.36% volume loss is employed for analysis in this study.

4.2.2 Geotechnical conditions

Geotechnical investigations, including in situ and laboratory tests, have revealed that the soil materials at the site predominantly consist of sandy ground (Migliazza et al., 2009). The upper layer is identified as sandy-gravel, while the layer beneath is characterized as silty-sandy. The geometry and geology of Milan Metro Line 1 are presented in Figure 7. Soil parameters employed in numerical simulation are shown in Table 2. More information of soil properties at Milan region can refer to Boldini et al. (2018), Fargnoli et al. (2013) and Fargnoli et al. (2015).

Table 2: Soil parameters in Milan Metro Line 1 (Migliazza et al., 2009).

Parameter, symbols and unit	Layer 1	Layer 2
Thickness t, m	<15	>15
Unit weight γ, kN/m^3	22	18
Cohesion c, kPa	0	0
Friction angle φ	30°	30°
Young's modulus E, MPa	100	75
Poisson's ratio v	0.3	0.3
Earth pressure at rest K_0	0.46	0.46

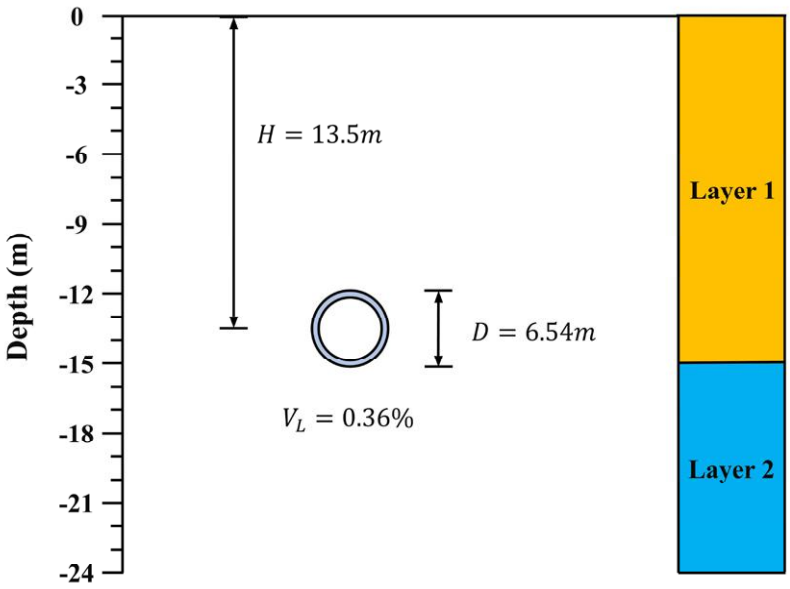

Figure 7: Geometry and geotechnical conditions of Milan Metro Line 1.

4.2.3 Results

The gap parameter was not recorded in this project. Instead, emphasis was placed on recording the volume loss of each tunnel cross-section. Numerical simulation results based on the proposed tunnel convergence patterns are compared with field data, as displayed in Figure 8. It reveals that the GSS troughs predicted by FEM are wider than that of field observations, which is consistent with the conclusions of many researchers such as Addenbrooke et al. (1997), Franzius et al. (2005), Grammatikopoulou et al. (2008) as well as Hejazi et al. (2008). Reasons can be contributed by the simplification of simulation procedure and soil constitutive models. Tunnel could experience ovalization in reality, but this was ignored in the simulation due to data limitation. With data of volume loss only, the actual tunnel convergence patterns cannot be accurately deduced, therefore, the tunnel periphery is assumed to maintain its original shape after convergence. This results in the discrepancy between the GSS trough predicted by the FEM and the one observed at the field. Furthermore, simplified 2D plane strain analysis does not consider the 3D effects of tunnelling and MC model cannot describe the non-linear response of soil behaviors.

However, despite the simplification of tunnelling simulation steps and 3D condition, the volume loss-equivalent method still provides a valuable probability analysis of GSS trough. Especially, under the tangent case, the simulated maximum GSS shows the closest agreement with field measurements. In this condition, the invert of the converged tunnel is tangent to its non-deformed profile, which indicates that deformation is primarily concentrated in the upper portion of the tunnel, while the invert experiences limited inward displacement.

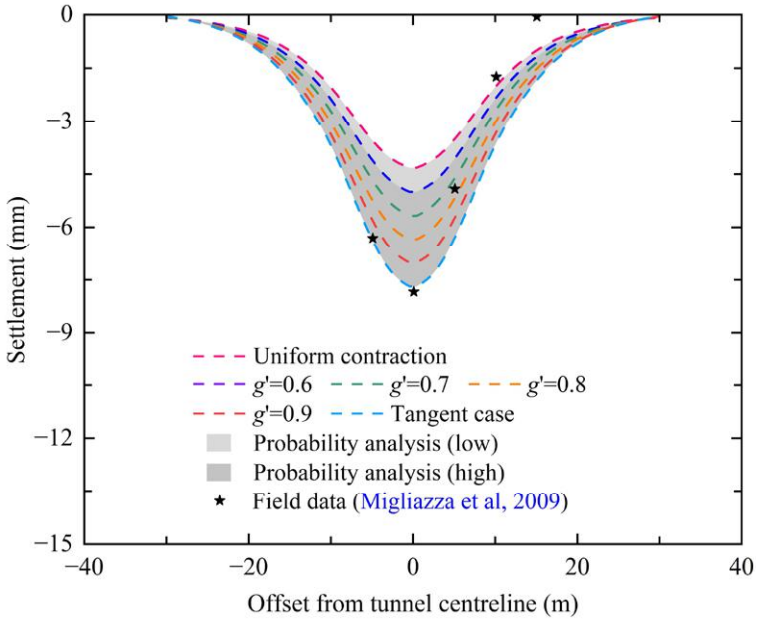

Figure 8: Transverse ground surface settlement of Milan Metro Line 1 Section 5-29.

4.3 ROME METRO LINE C

4.3.1 Background

Located in Rome, Italy, Rome Metro Line C extends from Monte Compatri-Pantano to San Giovanni, comprising two single-track tunnels (tunnel A and tunnel B). These two tunnels are constructed using EPBSM with an excavation diameter of 6.7m approximately. The external diameter of the liner is 6.4m. A cross-section near Carducci school is used for validation. This section (Section 11) has an axis depth of 25.4m. According to back-analysis, a volume loss of 0.48% can provide an accurate description of the monitored GSS trough (Miliziano and de Lillis, 2019).

4.3.2 Geotechnical conditions

Geotechnical investigations reveal that soil materials mainly consist of hard pyroclastic layers (Losacco and Viggiani, 2019). From ground surface, the encountered soil strata include: (1) 16m thickness man-made fill, characterized by medium dense to loss coarse-grained soil; (2) fluvial-alluvial deposit composed of clayey silt and sandy silt, with a maximum thickness of 18m; (3) pre-volcanic fluvial deposit, which is comprised of very dense silty sand, clayey silt, sandy gravel, and other materials. The physical and mechanical parameters of these materials are summarized in Table 3 and represented in Figure 9.

Table 3: Soil parameters in Rome Metro Line C Section 11 (Miliziano and de Lillis, 2019).

Layer	Description	$\gamma\ (kN/m^3)$	$c\ (kPa)$	$\varphi\ (°)$	$E\ (MPa)$	v	K_0
1	Coarse-grained soil	17.5	10	32	40	0.3	0.47
2	Clayey silt and sandy silt	17.5	15	32	22.5	0.3	0.68
3	Silty sand and clayey silt	20.0	10	35	52.5	0.3	0.64

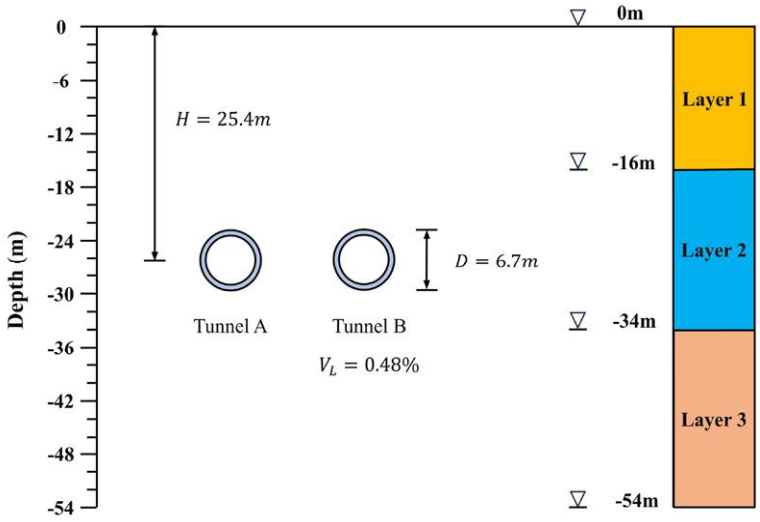

Figure 9: Geometry and geotechnical conditions of Rome Metro Line C.

4.3.3 Results

Following the same simulation procedure and using the equivalent volume loss, different tunnel convergence patterns are analyzed according to Equation 10 to 15 and Figure 4. GSS troughs predicted by DCM due to these tunnel convergence models are compared with field measurements in Figure 10. As can be seen, the obtained GSS troughs align well with field observations. The difference between field measurement and numerical results can primarily be attributed to the assumption that tunnel remains an ideal shape after convergence. As mentioned, for predicting GSS before tunnel excavation, the actual tunnel convergence pattern cannot be accurately deduced only from the volume loss data obtained from previous tunnel projects or back-analysis. In this condition, various typical tunnel convergence models are proposed based on field observations and centrifuge experiments, providing a probability analysis of GSS trough. The light grey region, which represents the phase from uniform convergence to slightly vertical displacement of liner ($g' = 0.6$), means a low probability of GSS occurrence since these conditions are idealistic. The dark grey area, which represents the intermediate states between slightly vertical displacement of liner ($g' = 0.6$) and the tangent situation ($g' = 1$), more aligns with the actual tunnel convergence situations and thus has higher GSS occurrence probability. More tunnel convergence measurement data can enhance the precision of fitting tunnel convergence functions and better characterize tunnel convergence, thereby improving the accuracy of GSS prediction.

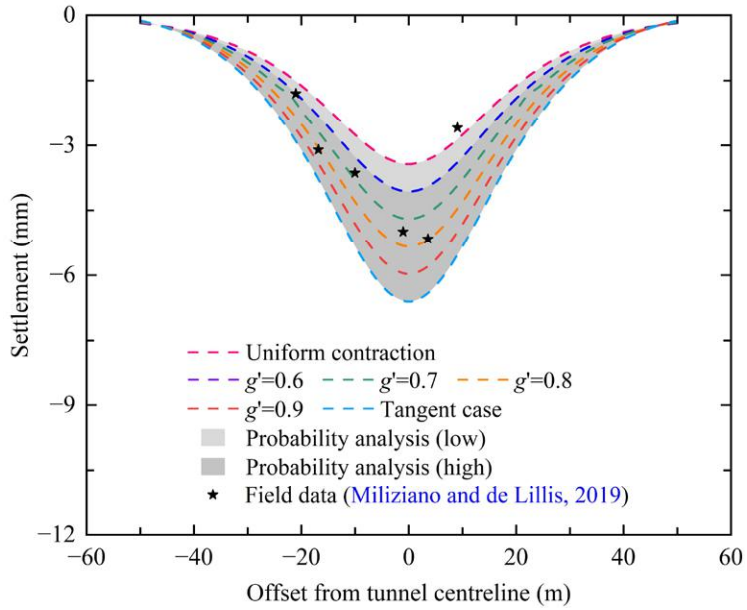

Figure 10: Transverse ground surface settlement of Rome Metro Line C Section 11.

5. PARAMETRIC STUDY

The parametric study is conducted based on Section 13+290 of Xi'an Metro Line 2, as previously studied. With the numerical model and soil parameters remain unchanged, variations are introduced in tunnel geometry and the extent of tunnel convergence. In other words, to isolate the effects of geotechnical variations, the soil parameters, including cohesion, friction angle, elastic modulus and Poisson's ratio, are kept constant. This ensures that the differences in the results are due to the alterations in tunnel geometry and convergence magnitude. The variations of tunnel geometry include changes in D and H. By changing these geometric parameters, the parametric study aims to understand their impacts on the maximum GSS. In addition, the numerical simulation results are also compared against empirical and analytical solutions.

5.1 EMPIRICAL AND ANALYTICAL METHODS

For the empirical method, Peck (1969) proposed that Gaussian curve can effectively fit the GSS trough. Based on field observations and engineering experience, he developed empirical formulas for tunnelling-induced GSS assessment shown as follows.

$$S_v = S_{max}\exp\left(\frac{-X^2}{2i^2}\right) \tag{16}$$

$$S_{max} = \frac{V_s}{2.5i} \tag{17}$$

$$V_s = \frac{V_L \pi D^2}{4} \tag{18}$$

Where S_v is the vertical surface settlement at the X distance from tunnel centreline, S_{max} is the maximum ground surface settlement that usually occurs above tunnel centreline, i is the point of inflexion of the settlement trough, V_s is the settlement volume per unit advancement, V_L is volume loss, D is tunnel diameter.

The position of inflexion point *i* has been modified by many researchers based on field observations or experimental findings. For instance, Knothe (1957) introduced Equation 19, indicating that *i* is associated with tunnel depth and soil friction angle. Herzog (1985) suggested Equation 20, drawing from observations in Germany. Equation 21 was introduced by Arioglu, (1992). Chakeri et al. (2013) proposed Equation 22 by averaging multiple empirical solutions for standard deviation consideration.

$$i = \frac{H}{\sqrt{2\pi}\tan\left(\frac{\pi}{4} - \frac{\varphi}{2}\right)} \tag{19}$$

$$i = 0.4H + 1.92 \tag{20}$$

$$i = 0.9\left(\frac{D}{2}\right)\left(\frac{H}{D}\right)^{0.88} \tag{21}$$

$$i = \frac{1}{7}\left[2.116H + R\left(0.9\left(\frac{H}{D}\right)^{0.88} + \left(\frac{H}{D}\right)^{0.8}\right) + 6.46\right] \tag{22}$$

In terms of analytical method, Loganathan and Poulos (1998) introduced elasticity-based analytical solutions. The validation of proposed formulas was verified in multiple tunnel projects ranging from very stiff to soft clay. Detailed representations are shown as follows.

$$S_v = 4(1-\nu)R^2\frac{H}{H^2+X^2}\frac{4gR+g^2}{4R^2}\exp\left[-\frac{1.38X^2}{(H+R)^2}\right] \tag{23}$$

Where g is the gap parameter, H is tunnel depth, R is tunnel radius, ν is Poisson's ratio of soil.

5.2 PARAMETERS IN GAP-CONTROLLED METHOD

According to tunnel convergence models presented in Figure 3, which adopt a constant gap parameter, Figure 11 shows the variation of S_{max} in response to changes in H, D, and g. As can be seen, the overall trend of numerical simulation results aligns well with empirical and analytical solutions. However, the uniform radial contraction of tunnel periphery (pattern 1) fails to accurately reflect tunnel deformations in real-world conditions due to its oversimplification. Among the empirical solutions, Arioglu (1992) predicts significantly higher S_{max} values than others, while Knothe (1957) provides comparatively lower values. The empirical solution 2 and 4 provide similar S_{max} estimations with the analytical solution. All three tend to overestimate S_{max} under loess conditions, where Xi'an Metro Line 2 is located. Compared to the analytical solution, numerical simulation results are more consistent with field measurements.

Figure 11 (a) illustrates that S_{max} nonlinearly reduces with the increasing of H, as deeper tunnels have smaller influence on the ground surface. The reduction rates in empirical and analytical solutions are faster than that calculated in numerical simulations. Figure 11 (b) shows that S_{max} increases as D increases. Similarly, the rate of increase in empirical and analytical solutions is faster compared to numerical simulations. This can be attributed to the relatively more comprehensive consideration of various influencing factors in numerical simulations, including soil properties and various tunnel convergence models. The relationship of g and S_{max} is depicted in Figure 11 (c). It shows that S_{max} increases with an increase in g, indicating that greater tunnel convergence can lead to more surface settlement. The increasing trend in numerical simulation results is in good agreement with empirical and analytical solutions, which both exhibit a nearly linear relationship.

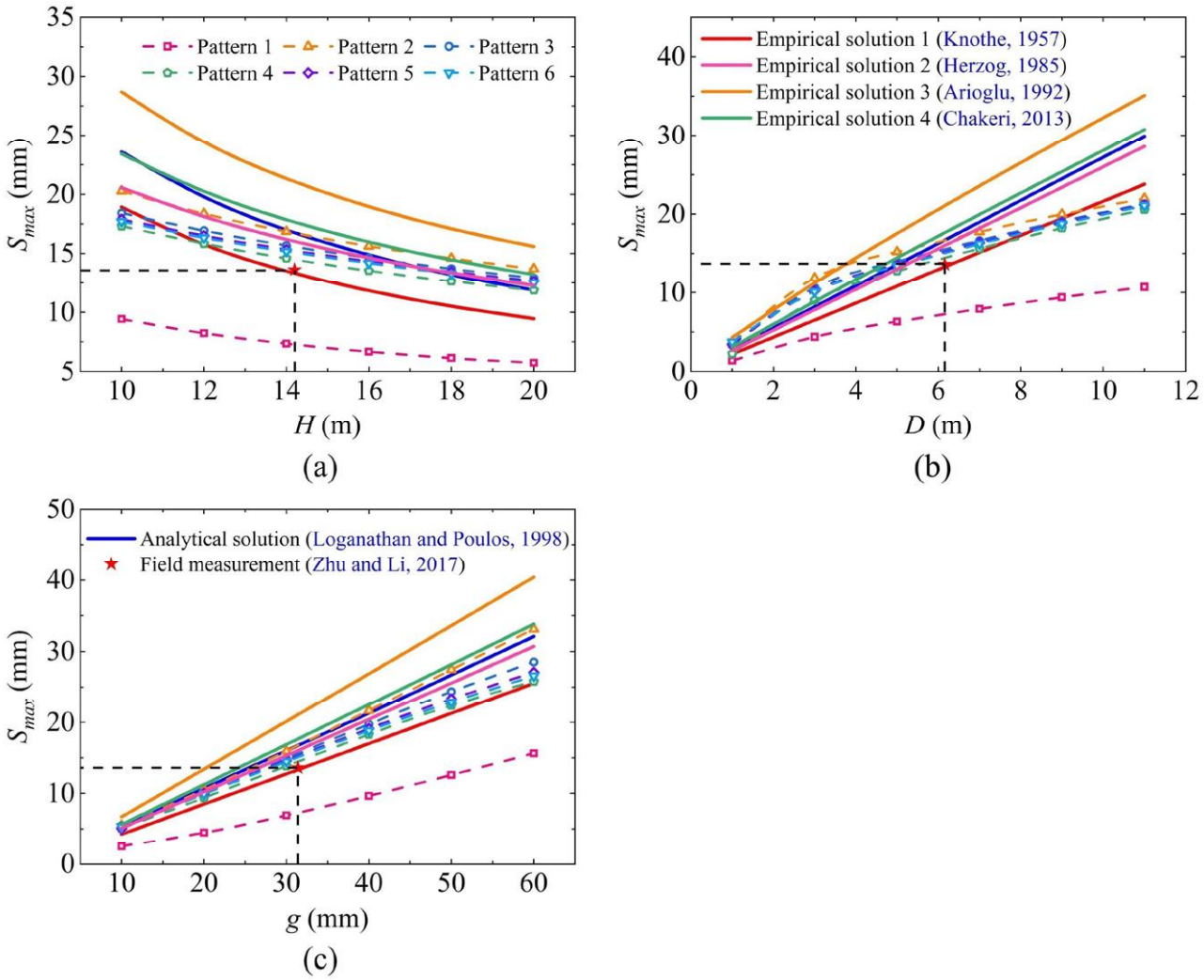

Figure 11: Variation of the maximum ground surface settlement with changing of (a) tunnel depth, (b) tunnel diameter and (c) gap parameter in the gap-controlled method.

5.3 PARAMETERS IN VOLUME LOSS-EQUIVALENT METHOD

Incorporating field observations and an analysis of the gap parameter at Section 13+290 of Xi'an Metro Line 2, a volume loss value of 1.02% is suggested (Zhu and Li, 2017). Follow the same procedure conducting the parametric analysis for tunnel convergence patterns based on the equivalent volume loss. Figure 12 displays the dependency of S_{max} on the variation of H, D and V_L, comparing various empirical solutions and convergence patterns. Overall, the numerical simulation results exhibit good agreement with empirical and analytical solutions. While the numerical results based on different convergence patterns align closely with the field measurement, the analytical and empirical solutions tend to overestimate S_{max} under the same V_L value.

Figure 12 (a) illustrates a reduction in S_{max} as H increases, with numerical simulations showing a slower rate of decrease compared to empirical and analytical solutions. Figure 12 (b) displays that S_{max} increases nonlinearly with increasing D, where empirical and analytical solutions exhibit a faster rate of increase relative to numerical simulations. Figure 12 (c) shows that S_{max} increases with increasing V_L, and the trend closely matches the approximate linear relationship observed in empirical and analytical solutions. In addition, the numerical simulation results basically envelop those of empirical and analytical solutions, with field measurement falling between them.

In summary, the volume loss-equivalent method provides a broader range of S_{max} compared with the gap-controlled method. This means the gap parameter is more important than the volume loss when evaluating S_{max} using DCM. In practice, acquiring the gap or volume loss parameters individually is inadequate to accurately capture actual tunnel deformation characteristics. If both parameters are obtained, the tunnel convergence model can be derived more accurately, thereby allowing for more accurate evaluation of GSS. Nonetheless, possessing information of just one of these two parameters still enables a preliminary estimation of S_{max} and GSS trough.

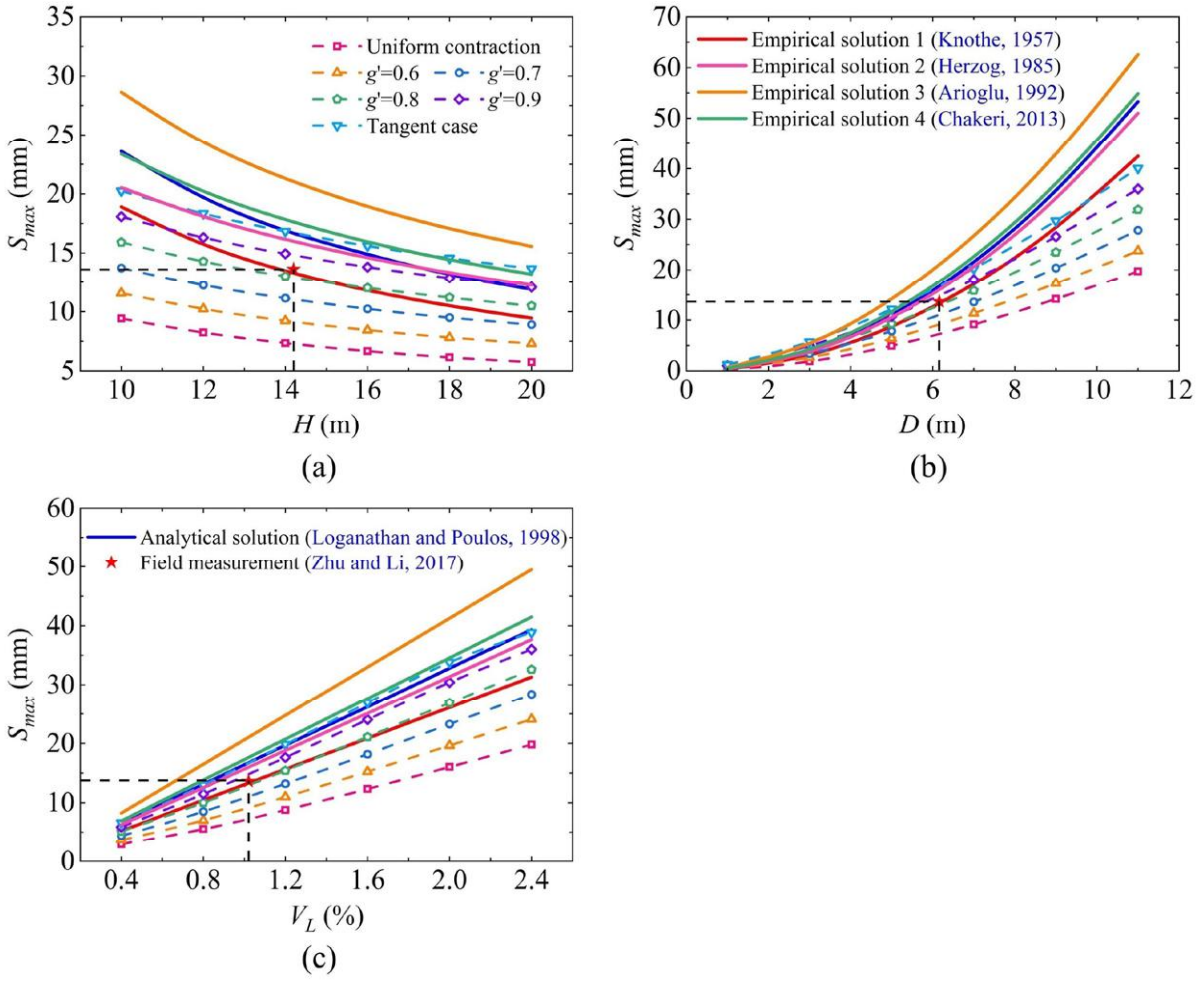

Figure 12: Variation of the maximum ground surface settlement with changing of (a) tunnel depth, (b) tunnel diameter and (c) volume loss in the volume loss-equivalent method.

6. DISCUSSION

6.1 ADVANTAGES AND LIMITATIONS OF PROPOSED METHOD

While the relationship between tunnel deformation and surface settlement has been studied by many researchers, this study extends these investigations by applying two numerical simulation-based approaches (the gap-controlled method and the volume loss-equivalent method) to systematically analyse the influence of tunnel convergence patterns on GSS troughs. The proposed 2D numerical method, based on the DCM, offers a probabilistic analysis of GSS during the initial stage of tunnel construction. Unlike conventional 3D numerical simulations that require detailed tunnelling information (e.g., excavation speed, thrust) and multiple sequential steps (e.g., application of face pressure, support removal, liner activation), the present method simplifies the process by directly incorporating tunnel convergence patterns. Figure 13 illustrates the steps of commonly used numerical methods for GSS evaluation. Figure 13 (a) outlines the analysis steps used in this study, while Figure 13 (b) and (c) summarize step-by-step 3D numerical simulation of tunnelling processes using FEM and FDM, respectively. As can be indicated, all methods start with establishing geostatic balance condition. Subsequently, 3D simulation of tunnelling activities follows multiple steps including applying face pressure, reducing support pressure and activating liner etc. These processes, while accurate, are often computationally intensive and time-consuming. In contrast, the proposed 2D numerical method requires fewer steps, thereby simplifying the simulation of tunnel excavation. By simplifying complicated tunnelling process into tunnel convergence patterns and incorporating geotechnical information along with data on the g or V_L, this method enables quick and probability analysis of GSS across various tunnel cross-sections. While maintaining satisfactory accuracy, this method effectively saves simulation time and improves computational efficiency. In addition, one potential engineering application is evaluating GSS in the early stages of a tunnel project utilizing limited information such as geotechnical properties, tunnel geometry, and tunnel convergence parameters (g or V_L). The determination of g and V_L is critical, as they significantly influence the derived tunnel convergence functions and tunnel convergence patterns.

Furthermore, different tunnelling methods, such as drill and blast, TBM, and New Austrian Tunnelling Method (NATM), can influence GSS in different ways. For instance, the drill and blast method has a higher potential for GSS due to the risk of over-excavation, as each blast can suddenly reduce stress at the excavation face, causing ground movement and localized settlement. In contrast, TBM tunnelling provides a more continuous and controlled excavation process (Wu et al., 2020; Yan et al., 2023). The managed excavation and immediate support installation result in lower GSS. For NATM, it tends to cause more significant and unpredictable GSS since the tunnel periphery is exposed for longer periods before the support is applied. For applying the method proposed in this study to tunnels constructed using the drill and blast approach as well as NATM, the tunnels need to be approximated as circle shapes, which can introduce errors due to the shape approximation. Additionally, in complex geotechnical conditions where the MC constitutive model fails to accurately describe soil behaviors, or when tunnel convergence is significant and exceeds the typical ranges, the proposed method need to be applied with caution.

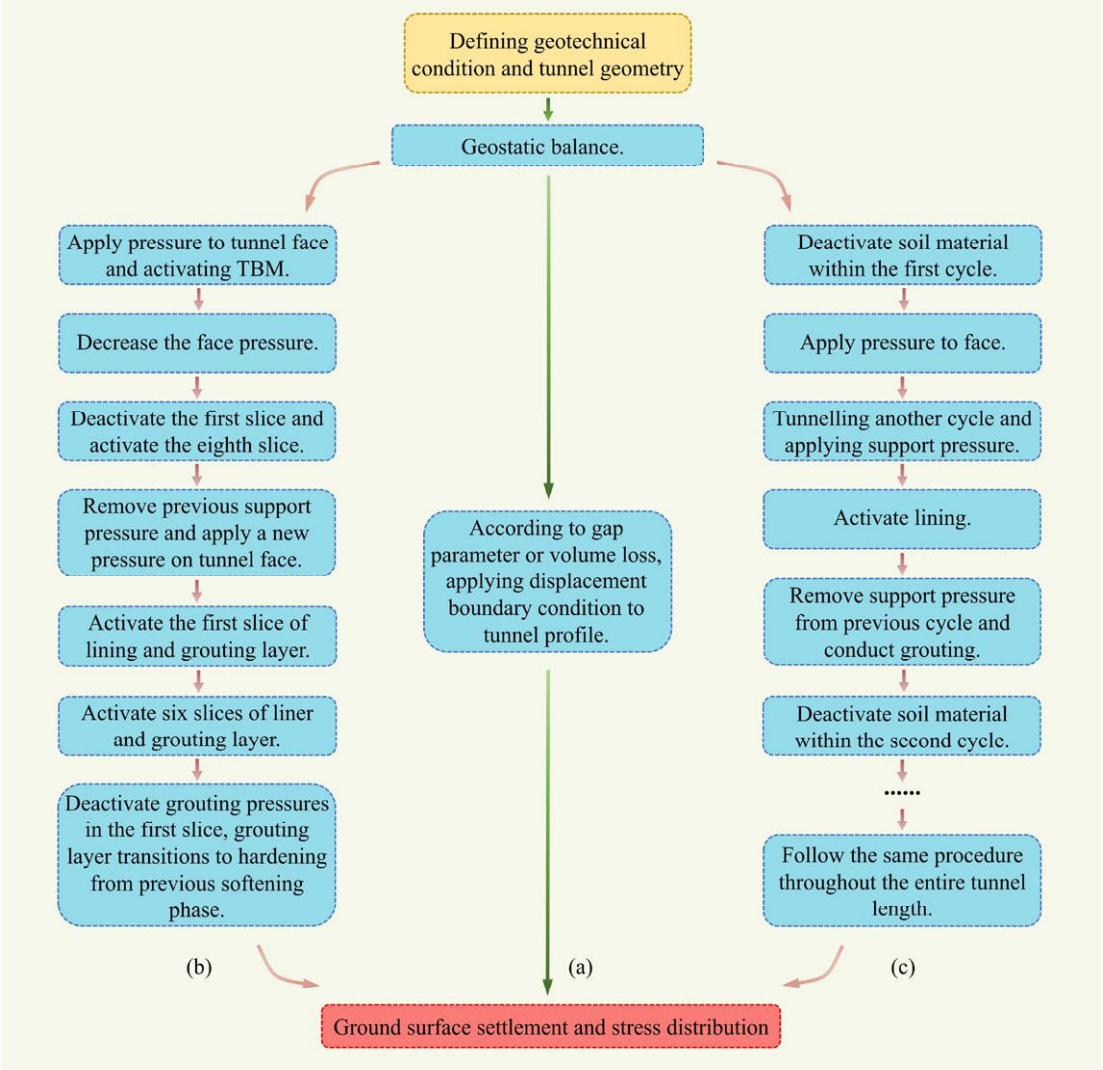

Figure 13: Comparison of proposed method with 3D simulation of tunnel excavation. (a) Simplified method in this study. (b) Step-by-step excavation in FEM (Li et al., 2019; Zhong et al., 2021). (c) Step-by-step excavation in FDM (Hao et al., 2022).

6.2 FUTURE DEVELOPMENT

In most tunnelling cases, ground deformation is relatively small, and the surrounding soil typically does not reach failure. Thus, the elastic response of soil is critical for analysing the GSS problem (Huang et al., 2017). The variation in Young's modulus contributes to changes in both the magnitude and width of ground settlement troughs (Zhang et al., 2021). The MC model, while widely used due to its simplicity, is primarily suited for problems involving large displacements where the nonlinearity of elastic behavior of soil is less important. This means the linear elastic response of MC model may falls short in accurately depicting soil behaviors in certain situations. For instance, over-consolidated clay exhibits highly nonlinear elastic before reaching failure (Grammatikopoulou et al., 2008). This nonlinearity cannot be captured by the linear elastic assumptions of the MC model, leading to potential inaccuracies in the analysis of GSS due to tunnelling in such soil conditions. Compared with MC, apply more advanced soil constitutive models such as Hardening Soil and Hardening Soil with Small Strain can enhance the assessment accuracy of tunnelling-induced GSS using DCM (Hejazi et al., 2008). Therefore, the development of User Subroutine (UMAT) is necessary for employing these models in ABAQUS. The efficacy of the proposed method in different soil constitutive models requires further exploration.

Furthermore, in numerical simulations, the assumption that soil material is homogenous and isotropic in each layer is often accepted for simplicity and efficiency. However, this assumption may not accurately reflect the complexity and variability of soil properties in real-world scenarios (Huang et al., 2015; Zhang et al., 2021). To address these challenges and achieve a more comprehensive analysis, it is suggested to incorporate a probability study. This can be achieved through the random fields of soil parameters, which considers the variability and uncertainty of soil properties. Consequently, it can offer more precise predictions of GSS associated with tunnelling activities.

7. CONCLUSION

This paper provides a simplified numerical method for the probability estimation of tunnelling-induced GSS. Various tunnel convergence models are proposed according to the g or V_L, respectively. Tunnel convergence is represented as a function of angle deviation. Employing these tunnel convergence functions in ABAQUS to make tunnel periphery experience targeted deformation, different resulting GSS troughs can be assessed. The region encompassed by these GSS troughs is considered as the probabilistic outcome of GSS. The effectiveness of proposed method is verified through case studies. From the analysis of results, the following conclusions can be made:

(1) Compared to 3D step-by-step tunnelling modelling that considers many factors such as face pressure, grouting pressure and grouting consolidation, the introduced approach eliminates the need for detailed material parameters and excavation specifics, thereby simplifying GSS analysis.

(2) The gap-controlled method is appropriate for instances where g is available. In cases that the V_L is obtained, DCM can operate on the principle of equivalent volume loss. Compared with the gap-controlled method, the volume loss-equivalent method provides a larger probabilistic region of GSS trough.

(3) The analytical method tends to overestimate S_{max} under loess conditions, as where Xi'an Metro Line 2 is located. In contrast, the proposed gap-controlled method can accurately describe the GSS trough both in shape and magnitude.

CRediT authorship contribution statement

Gang Niu: Conceptualisation, Software, Methodology, Writing - original draft. **Shaoeng Dai:** Data curation, Investigation, Methodology. **Yunhan Wang:** Validation, Visualisation. **Haoding Xu:** Validation. **Xuzhen He:** Supervision, Writing – review and editing.

8. REFERENCES

Addenbrooke, T. I., Potts, D. M., & Puzrin, A. M. (1997). The influence of pre-failure soil stiffness on the numerical analysis of tunnel construction. *Geotechniques*, *47*(3), 693–712.

Boldini, D., Losacco, N., Bertolin, S., & Amorosi, A. (2018). Finite Element modelling of tunnelling-induced displacements on framed structures. *Tunnelling and Underground Space Technology*, *80*, 222–231. https://doi.org/10.1016/j.tust.2018.06.019

Boubou, R., Emeriault, F., & Kastner, R. (2010). Artificial neural network application for the prediction of ground surface movements induced by shield tunnelling. *Canadian Geotechnical Journal*, *47*(11), 1214–1233. https://doi.org/10.1139/T10-023

Cao, L., Chen, X., Lu, D., Zhang, D., & Su, D. (2024). Theoretical prediction of ground settlements due to shield tunneling in multi-layered soils considering process parameters. *Underground Space (New)*, *16*, 29–43. https://doi.org/10.1016/j.undsp.2023.07.007

Cao, L., Zhang, D., Fang, Q., & Yu, L. (2020). Movements of ground and existing structures induced by slurry pressure-balance tunnel boring machine (SPB TBM) tunnelling in clay. *Tunnelling and Underground Space Technology*, 97. https://doi.org/10.1016/j.tust.2019.103278

Chakeri, H., Ozcelik, Y., & Unver, B. (2013). Effects of important factors on surface settlement prediction for metro tunnel excavated by EPB. *Tunnelling and Underground Space Technology*, 36, 14–23. https://doi.org/10.1016/j.tust.2013.02.002

Chen, R. P., Li, J., Kong, L. G., & Tang, L. jun. (2013). Experimental study on face instability of shield tunnel in sand. *Tunnelling and Underground Space Technology*, *33*, 12–21. https://doi.org/10.1016/j.tust.2012.08.001

Chen, R. P., Zhang, P., Kang, X., Zhong, Z. Q., Liu, Y., & Wu, H. N. (2019). Prediction of maximum surface settlement caused by earth pressure balance (EPB) shield tunneling with ANN methods. *Soils and Foundations*, *59*(2), 284–295. https://doi.org/10.1016/j.sandf.2018.11.005

Chen, Y. L., Shen, S. L., Zhou, A., & Zeng, Y. (2024). Novel model for evaluating ground settlement risk in slurry balance shield tunnel construction. *Tunnelling and Underground Space Technology*, *150*. https://doi.org/10.1016/j.tust.2024.105853

Cheng, C. Y., Dasari, G. R., Chow, Y. K., & Leung, C. F. (2007). Finite element analysis of tunnel-soil-pile interaction using displacement controlled model. *Tunnelling and Underground Space Technology*, *22*(4), 450–466. https://doi.org/10.1016/j.tust.2006.08.002

Chi, S.-Y., Chern, J.-C., & Lin, C.-C. (2001). Optimized back-analysis for tunneling-induced ground movement using equivalent ground loss model. *Tunnelling and Underground Space Technology* (Vol. 16).

Dias, D., & Kastner, R. (2013). Movements caused by the excavation of tunnels using face pressurized shields - Analysis of monitoring and numerical modeling results. *Engineering Geology*, *152*(1), 17–25. https://doi.org/10.1016/j.enggeo.2012.10.002

Do, N. A., Dias, D., Oreste, P., & Djeran-Maigre, I. (2014). 2D Tunnel Numerical Investigation: The Influence of the Simplified Excavation Method on Tunnel Behaviour. *Geotechnical and Geological Engineering*, *32*(1), 43–58. https://doi.org/10.1007/s10706-013-9690-y

Fargnoli, V., Boldini, D., & Amorosi, A. (2013). TBM tunnelling-induced settlements in coarse-grained soils: The case of the new Milan underground line 5. *Tunnelling and Underground Space Technology*, *38*, 336–347. https://doi.org/10.1016/j.tust.2013.07.015

Fargnoli, V., Gragnano, C. G., Boldini, D., & Amorosi, A. (2015). 3D numerical modelling of soil–structure interaction during EPB tunnelling. *Geotechnique*, *65*(1), 23–37. https://doi.org/10.1680/geot.14.P.091

Feng, X., Wang, P., Liu, S., Wei, H., Miao, Y., & Bu, S. (2022). Mechanism and Law Analysis on Ground Settlement Caused by Shield Excavation of Small-Radius Curved Tunnel. *Rock Mechanics and Rock Engineering*, *55*(6), 3473–3488. https://doi.org/10.1007/s00603-022-02819-6

Franza, A., Marshall, A. M., & Zhou, B. (2019). Greenfield tunnelling in sands: The effects of soil density and relative depth. *Geotechnique*, *69*(4), 297–307. https://doi.org/10.1680/jgeot.17.P.091

Franzius, J. N., Potts, D. M., & Burland, J. B. (2005). The influence of soil anisotropy and K0 on ground surface movements resulting from tunnel excavation. *Geotechnique*, *55*(3), 189–199.

Golpasand, M. R. B., Nikudel, M. R., & Uromeihy, A. (2016). Specifying the real value of volume loss (V L) and its effect on ground settlement due to excavation of Abuzar tunnel, Tehran. *Bulletin of Engineering Geology and the Environment*, 75(2), 485–501. https://doi.org/10.1007/s10064-015-0788-8

Grammatikopoulou, A., Zdravkovic, L., & Potts, D. M. (2008). The influence of previous stress history and stress path direction on the surface settlement trough induced by tunnelling. *Geotechnique*, *58*(4), 269–281. https://doi.org/10.1680/geot.2008.58.4.269Hao, D., Zhu, R., Wu, K., & Chen, R. (2022). Analysis of Ground Settlement Caused by Double-line TBM Tunnelling Under Existing Building. *Geotechnical and Geological Engineering*, *40*(2), 899–911. https://doi.org/10.1007/s10706-021-01934-5

Hejazi, Y., Dias, D., & Kastner, R. (2008). Impact of constitutive models on the numerical analysis of underground constructions. *Acta Geotechnica*, *3*(4), 251–258. https://doi.org/10.1007/s11440-008-0056-1

Hu, Y., Tang, H., Xu, Y., Lei, H., Zeng, P., Yao, K., & Dong, Y. (2024). Ground settlement and tunnel response due to twin-curved shield tunnelling in soft ground with small clear distance. *Journal of Rock Mechanics and Geotechnical Engineering*, *16*(8), 3122–3135. https://doi.org/10.1016/j.jrmge.2024.06.005

Huang, C., Du, H., Li, L., Ni, J., & Sun, Y. (2023). Application of tree-based methods in predicting the surface settlement arising from the tunnel excavation with large mix-shield. *Soils and Foundations*, *63*(6). https://doi.org/10.1016/j.sandf.2023.101379

Huang, H., Gong, W., Khoshnevisan, S., Juang, C. H., Zhang, D., & Wang, L. (2015). Simplified procedure for finite element analysis of the longitudinal performance of shield tunnels considering spatial soil variability in longitudinal direction. *Computers and Geotechnics*, *64*, 132–145. https://doi.org/10.1016/j.compgeo.2014.11.010

Huang, H. W., Xiao, L., Zhang, D. M., & Zhang, J. (2017). Influence of spatial variability of soil Young's modulus on tunnel convergence in soft soils. *Engineering Geology*, 228, 357–370. https://doi.org/10.1016/j.enggeo.2017.09.011

Huang, Z. K., Zhang, D. M., & Xie, X. C. (2022). A practical ANN model for predicting the excavation-induced tunnel horizontal displacement in soft soils. *Underground Space (China)*, *7*(2), 278–293. https://doi.org/10.1016/j.undsp.2021.07.009

Hussaine, S. M., & Mu, L. (2022). Intelligent Prediction of Maximum Ground Settlement Induced by EPB Shield Tunneling Using Automated Machine Learning Techniques. *Mathematics*, *10*(24). https://doi.org/10.3390/math10244637

Islam, M. S., & Iskander, M. (2021). Twin tunnelling induced ground settlements: A review. In *Tunnelling and Underground Space Technology* (Vol. 110). Elsevier Ltd. https://doi.org/10.1016/j.tust.2020.103614

Jallow, A., Ou, C. Y., & Lim, A. (2019). Three-dimensional numerical study of long-term settlement induced in shield tunneling. *Tunnelling and Underground Space Technology*, *88*, 221–236. https://doi.org/10.1016/j.tust.2019.02.021

Jin, D., Yuan, D., Ng, Y. C. H., & Pan, Y. (2022). Effect of an undercrossing tunnel excavation on an existing tunnel considering nonlinear soil-tunnel interaction. *Tunnelling and Underground Space Technology*, *130*. https://doi.org/10.1016/j.tust.2022.104571

Kim, D., Kwon, K., Pham, K., Oh, J. Y., & Choi, H. (2022). Surface settlement prediction for urban tunneling using machine learning algorithms with Bayesian optimization. *Automation in Construction*, *140*. https://doi.org/10.1016/j.autcon.2022.104331

Knothe, S. (1957). Observations of surface movements under influence of mining and their theoretical interpretation. *Proc European Conference on Ground Movement*, 210–218.

Lai, J., Zhou, H., Wang, K., Qiu, J., Wang, L., Wang, J., & Feng, Z. (2020). Shield-driven induced ground surface and Ming Dynasty city wall settlement of Xi'an metro. *Tunnelling and Underground Space Technology*, *97*. https://doi.org/10.1016/j.tust.2019.103220

Le, B. T., Nguyen, T. T. T., Divall, S., & Davies, M. C. R. (2023). A study on large volume losses induced by EBPM tunnelling in sandy soils. *Tunnelling and Underground Space Technology*, *132*. https://doi.org/10.1016/j.tust.2022.104847

Lee, K. M., Rowe, R. K., & Lo, K. Y. (1992). Subsidence owing to tunnelling. I. Estimating the gap parameter. *Can. Geotech. J.*, 29(6), 929–940.

Li, C., Zhong, Z., He, G., & Liu, X. (2019). Response of the ground and adjacent end-bearing piles due to side-by-side twin tunnelling in compound rock strata. *Tunnelling and Underground Space Technology*, *89*, 91–108. https://doi.org/10.1016/j.tust.2019.03.018

Lin, Q., Tian, Y., Lu, D., Gong, Q., Du, X., & Gao, Z. (2021). A prediction method of ground volume loss variation with depth induced by tunnel excavation. *Acta Geotechnica*, *16*(11), 3689–3707. https://doi.org/10.1007/s11440-021-01295-6

Ling, X., Kong, X., Tang, L., Zhao, Y., Tang, W., & Zhang, Y. (2022). Predicting earth pressure balance (EPB) shield tunneling-induced ground settlement in compound strata using random forest. *Transportation Geotechnics*, *35*. https://doi.org/10.1016/j.trgeo.2022.100771

Liu, L., Zhou, W., & Gutierrez, M. (2022). Effectiveness of predicting tunneling-induced ground settlements using machine learning methods with small datasets. *Journal of Rock Mechanics and Geotechnical Engineering*, *14*(4), 1028–1041. https://doi.org/10.1016/j.jrmge.2021.08.018

Loganathan, B. N., & Poulos, H. G. (1998). Analytical prediction for tunneling-induced ground movements in clays. *Geotech. Geoenviron. Eng.*, *124*(9), 846.

Losacco, N., & Viggiani, G. M. B. (2019). Class A prediction of mechanised tunnelling in Rome. *Tunnelling and Underground Space Technology*, *87*, 160–173. https://doi.org/10.1016/j.tust.2019.02.020

Ma, M., Liu, W., Qian, C., Deng, G., & Li, Y. (2016). Study of the train-induced vibration impact on a historic Bell Tower above two spatially overlapping metro lines. *Soil Dynamics and Earthquake Engineering*, *81*, 58–74. https://doi.org/10.1016/j.soildyn.2015.11.007

Ma, S., Liu, Y., Lv, X., Shao, Y., & Feng, Y. (2018). Settlement and Load Transfer Mechanism of Pipeline Due to Twin Stacked Tunneling with Different Construction Sequences. *KSCE Journal of Civil Engineering*, *22*(10), 3810–3817. https://doi.org/10.1007/s12205-018-0302-5

Mahmoodzadeh, A., Mohammadi, M., Daraei, A., Farid Hama Ali, H., Kameran Al-Salihi, N., & Mohammed Dler Omer, R. (2020). Forecasting maximum surface settlement caused by urban tunneling. *Automation in Construction*, *120*. https://doi.org/10.1016/j.autcon.2020.103375

Migliazza, M., Chiorboli, M., & Giani, G. P. (2009). Comparison of analytical method, 3D finite element model with experimental subsidence measurements resulting from the extension of the Milan underground. *Computers and Geotechnics*, *36*(1–2), 113–124. https://doi.org/10.1016/j.compgeo.2008.03.005

Miliziano, S., & de Lillis, A. (2019). Predicted and observed settlements induced by the mechanized tunnel excavation of metro line C near S. Giovanni station in Rome. *Tunnelling and Underground Space Technology*, *86*, 236–246. https://doi.org/10.1016/j.tust.2019.01.022

Miro, S., König, M., Hartmann, D., & Schanz, T. (2015). A probabilistic analysis of subsoil parameters uncertainty impacts on tunnel-induced ground movements with a back-analysis study. *Computers and Geotechnics*, *68*, 38–53. https://doi.org/10.1016/j.compgeo.2015.03.012

Moghaddasi, M. R., & Noorian-Bidgoli, M. (2018). ICA-ANN, ANN and multiple regression models for prediction of surface settlement caused by tunneling. *Tunnelling and Underground Space Technology*, *79*, 197–209. https://doi.org/10.1016/j.tust.2018.04.016

Möller, S. C., & Vermeer, P. A. (2008). On numerical simulation of tunnel installation. *Tunnelling and Underground Space Technology*, *23*(4), 461–475. https://doi.org/10.1016/j.tust.2007.08.004

Niu, G., He, X., Xu, H., & Dai, S. (2023). Tunnelling-induced ground surface settlement: A comprehensive review with particular attention to artificial intelligence technologies. *Natural Hazards Research*. https://doi.org/10.1016/j.nhres.2023.11.002

Noubissi, C., Taherzadeh, R., Puel, G., & Lopez-Caballero, F. (2024). An Optimized methodology of back-analysis and sensitivity analysis for the settlement evaluation: Case study on a TBM on the Metro Line 12 extension in the Paris region. In *Computers and Geotechnics* (Vol. 167). Elsevier Ltd. https://doi.org/10.1016/j.compgeo.2023.106043

Paraskevopoulou, C., & Diederichs, M. (2018). Analysis of time-dependent deformation in tunnels using the Convergence-Confinement Method. *Tunnelling and Underground Space Technology*, *71*, 62–80. https://doi.org/10.1016/j.tust.2017.07.001

Park, K. H. (2005). Analytical solution for tunnelling-induced ground movement in clays. *Tunnelling and Underground Space Technology*, *20*(3), 249–261. https://doi.org/10.1016/j.tust.2004.08.009

Peck, R. B. (1969). Deep excavations and tunneling in soft ground. *Proceedings of the 7th International Conference on Soil Mechanics and Foundation Engineering*, 225–290.

Peng, J. bing, Huang, Q. bing, Hu, Z. ping, Wang, M. xiao, Li, T., Men, Y. ming, & Fan, W. (2017). A proposed solution to the ground fissure encountered in urban metro construction in Xi'an, China. *Tunnelling and Underground Space Technology*, *61*, 12–25. https://doi.org/10.1016/j.tust.2016.09.002

Pourtaghi, A., & Lotfollahi-Yaghin, M. A. (2012). Wavenet ability assessment in comparison to ANN for predicting the maximum surface settlement caused by tunneling. *Tunnelling and Underground Space Technology*, *28*(1), 257–271. https://doi.org/10.1016/j.tust.2011.11.008

Rowe, R. K., Lo, K. Y., & Kack, G. J. (1983). A method of estimating surface settlement above tunnel constructed in soft ground. *Canadian Geotechnical Journal*, *20*, 11–22.

Russo, G., Corbo, A., Cavuoto, F., & Autuori, S. (2015). Artificial Ground Freezing to excavate a tunnel in sandy soil. Measurements and back analysis. *Tunnelling and Underground Space Technology*, *50*, 226–238. https://doi.org/10.1016/j.tust.2015.07.008

Santos, O. J., & Celestino, T. B. (2008). Artificial neural networks analysis of São Paulo subway tunnel settlement data. *Tunnelling and Underground Space Technology*, *23*(5), 481–491. https://doi.org/10.1016/j.tust.2007.07.002

Shahin, H. M., Nakai, T., & Okuno, T. (2019). Numerical study on 3D effect and practical design in shield tunneling. *Underground Space (China)*, *4*(3), 201–209. https://doi.org/10.1016/j.undsp.2019.01.002

Shahin, H. M., Nakai, T., Zhang, F., Kikumoto, M., & Nakahara, E. (2011). Behavior of ground and response of existing foundation due to tunneling. *Soils and Foundations*, *51*(3), 395–409.

Shen, S. L., Elbaz, K., Shaban, W. M., & Zhou, A. (2022). Real-time prediction of shield moving trajectory during tunnelling. *Acta Geotechnica*, *17*(4), 1533–1549. https://doi.org/10.1007/s11440-022-01461-4

Shen, S. L., Wu, H. N., Cui, Y. J., & Yin, Z. Y. (2014). Long-term settlement behaviour of metro tunnels in the soft deposits of Shanghai. *Tunnelling and Underground Space Technology*, *40*, 309–323. https://doi.org/10.1016/j.tust.2013.10.013

Shiau, J., & Sams, M. (2019). Relating volume loss and greenfield settlement. *Tunnelling and Underground Space Technology*, *83*, 145–152. https://doi.org/10.1016/j.tust.2018.09.041

Song, X., Wu, H. N., Meng, F. Y., Chen, R. P., & Cheng, H. Z. (2023). Soil arching evolution caused by shield tunneling in deep saturated ground. *Transportation Geotechnics*, *40*. https://doi.org/10.1016/j.trgeo.2023.100966

Tang, L., & Na, S. H. (2021). Comparison of machine learning methods for ground settlement prediction with different tunneling datasets. *Journal of Rock Mechanics and Geotechnical Engineering*, *13*(6), 1274–1289. https://doi.org/10.1016/j.jrmge.2021.08.006Verruijt, A., & Booker, J. R. (1996). *Surface settlements due to deformation of a tunnel in an elastic half plane*.

Vu, M. N., Broere, W., & Bosch, J. (2016). Volume loss in shallow tunnelling. *Tunnelling and Underground Space Technology*, 59, 77–90. https://doi.org/10.1016/j.tust.2016.06.011

Wu, H. N., Shen, S. L., Chen, R. P., & Zhou, A. (2020). Three-dimensional numerical modelling on localised leakage in segmental lining of shield tunnels. *Computers and Geotechnics*, *122*. https://doi.org/10.1016/j.compgeo.2020.103549

Xie, X., Tian, H., Zhou, B., & Li, K. (2021). The life-cycle development and cause analysis of large diameter shield tunnel convergence in soft soil area. *Tunnelling and Underground Space Technology*, *107*. https://doi.org/10.1016/j.tust.2020.103680

Yan, T., Shen, S. L., & Zhou, A. (2023). GFII: A new index to identify geological features during shield tunnelling. *Tunnelling and Underground Space Technology*, *142*. https://doi.org/10.1016/j.tust.2023.105440

Yang, W., Zheng, J., Zhang, R., & Liu, H. (2021). An empirical model for characterizing 3D deformation at the face of shield tunnel in soft clay. *Tunnelling and Underground Space Technology*, 112. https://doi.org/10.1016/j.tust.2021.103862

Yang, W., Zheng, J., Zhang, R., & Liu, H. (2022). An analytical method for predicting equivalent gap parameter induced by 3D deformation at the face of shield tunnel in soft clay. *Tunnelling and Underground Space Technology*, 130. https://doi.org/10.1016/j.tust.2022.104736

Zakhem, A. M., & El Naggar, H. (2019). Effect of the constitutive material model employed on predictions of the behaviour of earth pressure balance (EPB) shield-driven tunnels. *Transportation Geotechnics*, *21*. https://doi.org/10.1016/j.trgeo.2019.100264

Zareifard, Mohammad Reza. (2019). Ground response curve of deep circular tunnel in rock mass exhibiting Hoek–Brown strain-softening behaviour considering the dead weight loading. *European Journal of Environmental and Civil Engineering*, 1–31.

Zhang, J. Z., Huang, H. W., Zhang, D. M., Zhou, M. L., Tang, C., & Liu, D. J. (2021). Effect of ground surface surcharge on deformational performance of tunnel in spatially variable soil. *Computers and Geotechnics*, *136*. https://doi.org/10.1016/j.compgeo.2021.104229

Zhang, J., Phoon, K. K., Zhang, D., Huang, H., & Tang, C. (2021). Deep learning-based evaluation of factor of safety with confidence interval for tunnel deformation in spatially variable soil. *Journal of Rock Mechanics and Geotechnical Engineering*, 13(6), 1358–1367. https://doi.org/10.1016/j.jrmge.2021.09.001

Zhang, K., Lyu, H. M., Shen, S. L., Zhou, A., & Yin, Z. Y. (2020). Evolutionary hybrid neural network approach to predict shield tunneling-induced ground settlements. *Tunnelling and Underground Space Technology*, *106*. https://doi.org/10.1016/j.tust.2020.103594

Zhang, P., Wu, H. N., Chen, R. P., Dai, T., Meng, F. Y., & Wang, H. B. (2020). A critical evaluation of machine learning and deep learning in shield-ground interaction prediction. *Tunnelling and Underground Space Technology*, *106*. https://doi.org/10.1016/j.tust.2020.103593

Zhang, P., Wu, H. N., Chen, R. P., & Chan, T. H. T. (2020). Hybrid meta-heuristic and machine learning algorithms for tunneling-induced settlement prediction: A comparative study. *Tunnelling and Underground Space Technology*, *99*. https://doi.org/10.1016/j.tust.2020.103383

Zhang, Z., & Huang, M. (2012). Boundary element model for analysis of the mechanical behavior of existing pipelines subjected to tunneling-induced deformations. *Computers and Geotechnics*, *46*, 93–103. https://doi.org/10.1016/j.compgeo.2012.06.001

Zhang, Z., Huang, M., & Zhang, M. (2011). Theoretical prediction of ground movements induced by tunnelling in multi-layered soils. *Tunnelling and Underground Space Technology*, *26*(2), 345–355. https://doi.org/10.1016/j.tust.2010.11.005

Zhong, Z., Li, C., Liu, X., Fan, Y., & Liang, N. (2021). Analysis of ground surface settlement induced by the construction of mechanized twin tunnels in soil-rock mass mixed ground. *Tunnelling and Underground Space Technology*, *110*. https://doi.org/10.1016/j.tust.2020.103746

Zhou, J., Qi, H., Peng, K., Zhang, Y., & Khandelwal, M. (2024). Comprehensive review and future perspectives on prediction and mitigation of tunnel-induced ground settlement: A bibliometric analysis and methodological overview (2002–2022). *Tunnelling and Underground Space Technology*, *154*. https://doi.org/10.1016/j.tust.2024.106081

Zhu, B., Zhang, P., Lei, M., Wang, L., Gong, L., Gong, C., & Chen, F. (2023). Improved analytical solution for ground movements induced by circular tunnel excavation based on ground loss correction. *Tunnelling and Underground Space Technology*, *131*. https://doi.org/10.1016/j.tust.2022.104811

Zhu, C., & Li, N. (2017). Prediction and analysis of surface settlement due to shield tunneling for Xi'an Metro. *Canadian Geotechnical Journal*, *54*(4), 529–546. https://mc06.manuscriptcentral.com/cgj-pubs